DNA Nanotechnology

DOI: 10.1002/anie.201307113

Crystallization of DNA-Capped Gold Nanoparticles in High-Concentration, Divalent Salt Environments**

Shawn J. Tan, Jason S. Kahn, Thomas L. Derrien, Michael J. Campolongo, Mervin Zhao, Detlef-M. Smilgies, and Dan Luo**

Abstract: *The multiparametric nature of nanoparticle self-assembly makes it challenging to circumvent the instabilities that lead to aggregation and achieve crystallization under extreme conditions. By using non-base-pairing DNA as a model ligand instead of the typical base-pairing design for programmability, long-range 2D DNA–gold nanoparticle crystals can be obtained at extremely high salt concentrations and in a divalent salt environment. The interparticle spacings in these 2D nanoparticle crystals can be engineered and further tuned based on an empirical model incorporating the parameters of ligand length and ionic strength.*

One of the fundamental goals of nanotechnology is the self-assembly of nanoparticles into highly ordered nanostructures towards a new generation of advanced materials for optoelectronic devices as well as sensing and diagnostic applications. However, the multi-parametric process of self-assembly poses many challenges for achieving crystallization reliably over a broad and robust set of conditions necessary for real-world applications, such as in aqueous solutions with high salt concentration or with multivalent ions.

In the past decade, DNA has garnered significant attention as a designer ligand for the directed self-assembly of nanoparticle crystals, owing to its unique programmability afforded by Watson–Crick base-pairing.[1–6] The complexity of base-pairing, coupled with the remarkable length and sequence control inherent in DNA synthesis, offers versatility and precision in the organization of DNA–nanoparticle (DNA-NP) colloidal crystals. Base-pairing DNA has been employed for crystallization with considerable success, with specific base-pairing affording significant control over lattice structure and melting properties of DNA-NP crystals.[1–6]

Correspondingly, investigations to elucidate the underlying mechanisms and interactions of soft nanoparticle crystallization have typically revolved around base-pairing DNA ligands, and thus within a limited range of ionic strengths (ISs) in monovalent salt solutions, so as to maintain the integrity of base-pairing.[1,2,7–10] However, to transition into real-world applications, it is imperative to address the delicate balance in the crystallization of soft nanoparticles and biomolecules that make them extremely susceptible to instabilities leading to aggregation. A grand challenge in crystallization is tuning the underlying interactions that drive this multiparametric process. Yet to date, there remains a dearth of information on nanoparticle crystallization at a large range of IS such as at high salt concentration or multivalent salt environments, largely because of the susceptibility of nanoparticles to aggregation in such environments.

Here, we report the remarkable capacity for non-base-pairing DNA-NPs to crystallize under an extreme range of ISs solutions. We chose Mg^{2+} as the divalent counterion for our studies, as it is a critical component in biological systems and also plays a key role in maintaining structural stability in DNA nanotechnology.[11–13] Extreme high salt conditions (up to 2.1 M NaCl) were also investigated for their importance in expanding the utility of nanoparticle crystals in sensing and diagnostic applications to include processes involving high ISs. Our results present a paradigm shift by vastly expanding the utility of DNA-NP assemblies beyond typical base-pairing designs or monovalent salt conditions that have been well-investigated.[14–16] Also, the crystallization phenomena observed will be extendable to other polyelectrolyte-based soft-sphere systems.

Our studies were performed with a DNA-NP system comprising of 14 nm gold nanoparticles (AuNPs) densely capped with polythymine (polyT) ligands of variable lengths (Figure 1). Non-base-pairing DNA serves as a model ligand

[*] Dr. S. J. Tan,[+] Dr. M. J. Campolongo, Prof. D. Luo
Department of Biomedical Engineering, Cornell University
Ithaca, NY 14853 (USA)
E-mail: jt394@cornell.edu
dl79@cornell.edu
Dr. D.-M. Smilgies
Cornell High Energy Synchrotron Source, Cornell University
Ithaca, NY 14853 (USA)
J. S. Kahn, T. L. Derrien, M. Zhao
Department of Biological and Environmental Engineering
Cornell University, Ithaca, NY 14853 (USA)
Prof. D. Luo
Kavli Institute at Cornell, Cornell University
Ithaca, NY 14853 (USA)
[+] Current Address:
Institute of Materials Research and Engineering
3 Research Link, Singapore 117602 (Singapore)

[**] We thank Lois Pollack and her group for discussions on DNA-counterion interactions. S.J.T. is a recipient of the National Science Scholarship awarded by A-STAR, Singapore. J.S.K. is supported by the DOE-OSGFP, made possible in part by the American Recovery and Reinvestment Act of 2009, administered by ORISE-ORAU under contract number DE-AC05-06OR23100. T.L.D. and M.J.C. are supported by the IGERT Program of the National Science Foundation under agreement number DGE-0903653, administered by NBTC at Cornell University. D.L. acknowledges financial support from NYSTAR and an NSF CAREER award (grant number 0547330). CHESS is supported by the NSF and NIH/NIGMS through an NSF award (grant number DMR-0936384). This work also made use of the Cornell Center for Materials Research shared facilities, which are supported through the NSF MRSEC program (DMR-1120296).

Supporting information for this article is available on the WWW under http://dx.doi.org/10.1002/anie.201307113.

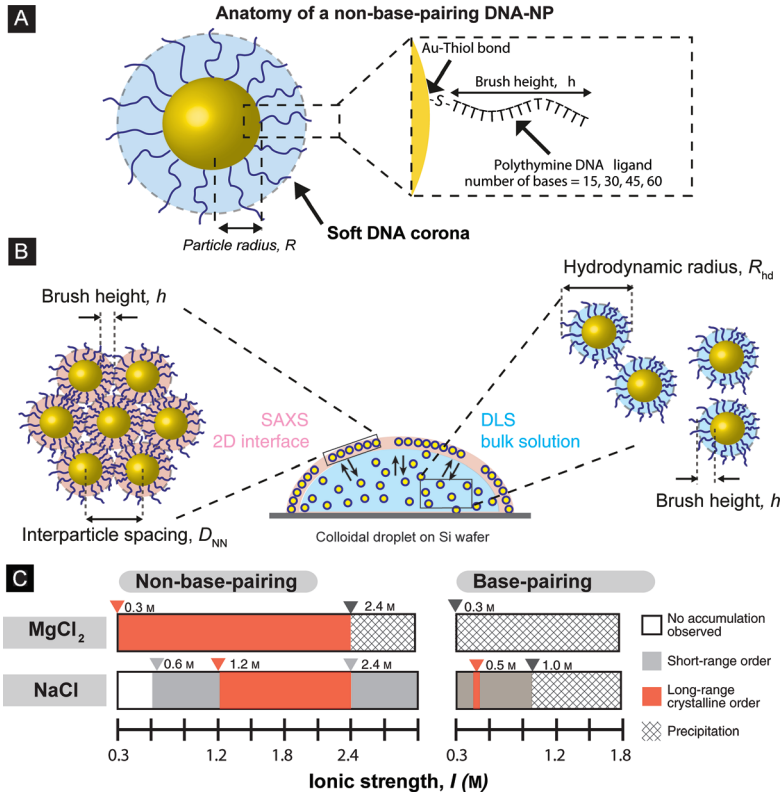

Figure 1. A) Gold nanoparticles capped with a soft non-base-pairing DNA corona comprising of polythymine ligands with length *n*. B) Investigation of DNA-NP interactions at the air–water interface of a sessile droplet. parSAXS provided information on the crystalline order, interparticle spacing (D_{NN}), and the effective brush height (h) at the air–water interface. C) The interfacial behavior of base-pairing DNA-NPs (with an 8-base palindromic sequence) and non-base-pairing DNA for different IS of NaCl and $MgCl_2$ is summarized based on experimental observations at the optimal ligand length. With base-pairing DNA-NPs, precipitation occurred at the lowest IS of Mg^{2+} tested. The behavior of base-pairing DNA-NPs in NaCl is adapted from literature for comparison.[10]

because it eliminates crystallization driven by specific Watson–Crick base-pairing while affording precise control over a wide range of brush heights in extreme IS solutions. The choice of polyT ligands avoided secondary structure formation such as hairpin loops in the DNA corona.

We used parallel small-angle x-ray scattering (parSAXS) which enabled us to uniquely probe the ordering phenomenon at the air–water interface independent of substrate effects.[10] Notably, our system is fully equilibrated (free particle exchange between bulk solution and Gibbs layer) and friction-free (in liquid rather than on a solid substrate). A droplet of polyT-DNA-capped AuNPs was deposited in a sealed chamber with a reservoir at the same salt concentration, in order to maintain equilibrium vapor pressure in the chamber and thus to stabilize the droplet volume and minimize far-from-equilibrium drying effects (see the Supporting Information).[10] The scattering spectra at the interface of the droplet were captured in real time and in situ for non-base-pairing DNA-NPs across a range of ISs of monovalent NaCl and divalent $MgCl_2$ solutions.

Here, we observed the remarkable capacity for non-base-pairing DNA-NPs to crystallize in high IS solutions of mono- and divalent salts—two environments that typically lead to aggregation of colloidal nanoparticles. Notably, crystalline monolayers of soft DNA-NPs were achieved over a broad range of ISs for NaCl and $MgCl_2$ (Figure 1c). As a comparison, our earlier work on base-pairing DNA-NPs indicated that crystallization occurred within a narrow range of ISs for monovalent NaCl, with precipitation quickly occurring from an IS_{NaCl} of 1.0 M and above.[9,10] Since base-pairing interactions dominate the assembly process, DNA-NPs aggregated and precipitated beyond this threshold of ionic strengths.[16] This problem is accentuated in divalent salt environments, with base-pairing DNA-NPs aggregating in $MgCl_2$ solutions even at the lowest tested IS_{MgCl2} 0.3 M that was studied. Hence, it is important to highlight that non-base-pairing DNA is critical for investigating soft nanoparticle crystallization in extreme salt concentration and multivalent salt environments.

In the absence of salt, electrostatic repulsion amongst non-base-pairing DNA ligands dominates the interactions between DNA-NPs. At the low IS_{NaCl} of a 0.3 M NaCl solution, insufficient charge screening resulted in sparse packing of DNA-NPs at the interface so that not even short-range order was observed (Figure 2). Short-range order was evident from an IS_{NaCl} of a 0.9 M NaCl solution and above with crystalline order emerging from 1.2 M onwards. In contrast, short-range order among DNA-NPs was observed already from the lowest tested IS_{MgCl2} of a 0.3 M solution. Notably, the brush height of DNA-NPs, estimated by the d-spacing from first-order Bragg peaks (see the Supporting Information), was significantly reduced in $MgCl_2$ to about half of that in NaCl, even at the same IS. These results are consistent with previous studies performed on single-stranded DNA molecules,[17] which indicated that Mg^{2+} was dramatically more effective at charge screening of DNA than Na^+ even at the same IS. Effective charge screening is necessary to mediate the repulsive electrostatic forces of the DNA-NPs and allow for assembly into higher-ordered structures.[18]

The scattering spectra shown in Figure 2 reveal the effect of ligand length and the IS on the crystallization of non-base-pairing DNA-NPs. Long-range order was typically observed in ligand lengths from 30 to 60 bases, and IS_{NaCl} from 1.2 M to 2.1 M solutions or IS_{MgCl2} from 0.3 M to 2.1 M solutions (see Figure 2). We posit that long-range order is achieved at an optimal ligand length for a given salt concentration because of a balance of antagonistic effects: 1) longer ligands increase the hydrodynamic size as shown from dynamic light scattering (DLS; see the Supporting Information) data, resulting in a larger volume fraction confined at the interface. This favors nanoparticle ordering to maximize the free volume at the air–

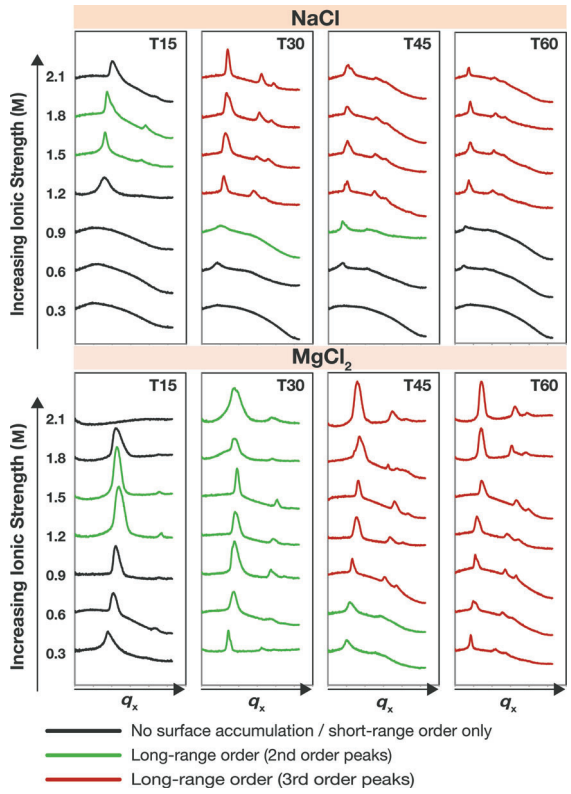

Figure 2. Scattering spectra for non-base-pairing DNA-NPs, densely capped with polythymine ligands of variable lengths of 15, 30, 45, 60 bases, organized at the air–water interface at different IS of NaCl and $MgCl_2$. First-order peaks in the scattering spectra indicate nanoparticle monolayers with short-range order (black lines), whereas second-order (green lines) and third-order peaks (red lines) indicate long-range crystalline order.

water interface;[19,20] 2) conversely, longer ligands demand greater conformational freedom which compromises the ordering at the interface. Our results suggest that the relative contributions of these effects are different in monovalent and divalent salt environments.

To elucidate the mechanism behind the formation of 2D crystals with long-range order as the salt concentration increased, we used a combination of parSAXS and DLS to probe the disparate behavior of DNA-NPs at the air–water interface and in bulk solution in response to the IS. Notably, while the brush height of the DNA-NPs in bulk solution increased in the high salt regime, the brush height decreased at the air–water interface with increasing IS (Figure S5). This indicated that the accumulation and ordering of NPs at the interface was not driven by the brush deformation from an increasing IS, but rather resulted in the form of the classic Gibbs mechanism[21,22] to alleviate the increase in surface tension from an increasing salt concentration.[23,24]

Furthermore, the grain sizes decreased with ligand length because of the need of greater conformational freedom for longer ligands. In the case of $MgCl_2$, specific interactions of the divalent Mg^{2+} counterion may have limited this demand and instead favored the ordering of DNA-NPs with increasing ligand length and volume fraction. As a result, an optimal grain size of 940 nm was achieved for $MgCl_2$ environments at the longest ligand length of 60 bases (see the Supporting Information). This optimal grain size is much larger than that for NaCl (630 nm), and is also dramatically larger than the previous grain size of 360 nm for base-pairing DNA-NPs.[10] Furthermore, these DNA-NP superlattices assembled at the interface could be transferred onto a substrate in an additional step (see Figure S8 in the Supporting Information).

The high monodispersity and precise length tunability of DNA make it an ideal ligand for investigating, modelling, and engineering soft nanoparticle assemblies across a broad range of ligand lengths.[25] With non-base-pairing DNA as a ligand, we were able to extend the utility of DNA-NPs into the high salt regime and in divalent salt environments that was previously inaccessible to other soft nanoparticle systems. With this new set of information, we modelled the effect of ligand length and IS on the brush height based on a modified Daoud–Cotton (mDC) model. Details of the model can be found in the Supporting Information. With known ligand densities for each DNA-NP sample calculated from fits to our NaCl data (see Figure S6), we assigned K_2, β, and γ as empirical fitting parameters for IS (I) and ligand length (N) to DNA brush height [Eq. (1)],

$$\frac{h}{R} = \left(1 + K_2 N b R^{-1} \left(\sigma I^{-\beta} N^{-\gamma}\right)^{1/3}\right)^{3/5} - 1 \qquad (1)$$

where h is the DNA brush height, R is the nanoparticle radius, K_2 is a proportionality constant, N is the number of bases, b is the length per base (0.65 nm per base for ssDNA), and σ is the DNA ligand density (chains per square-nanometer). Surprisingly, the DNA brush height in $MgCl_2$ fits the mDC model remarkably well, with values of $K_2 = 1.41$, $\beta = 1$, and $\gamma = 0$ and a reduced $-\chi^2$ of 0.9 (Figure 3). In comparison, the corresponding values for monovalent Na^+ counterions are $K_1 = 2.10$, $\beta = 1$, and $\gamma = 0$, which are consistent with the mDC model we previously reported.[10] The model developed here can serve as the foundation for designing ordered DNA-NP crystals in the presence of divalent salts. We note that Guo

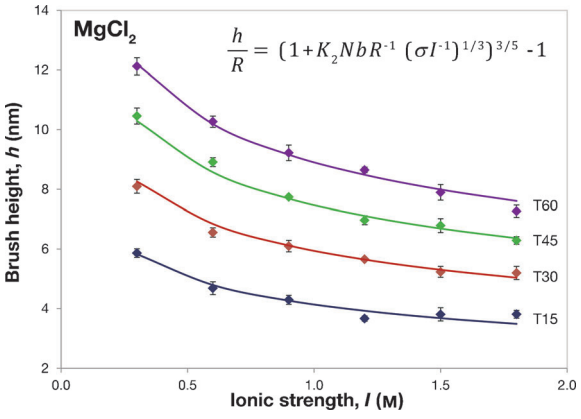

Figure 3. Brush height of DNA-NPs for different ligand lengths across a range of IS in $MgCl_2$. Points represent experimental data, lines represent theoretical fits to the proposed models. Average brush height and error bars were computed from the interparticle spacing obtained from multiple points at the air–water interface along the droplet profile. Solid lines were model fits while points are experimental data.

and Ballauff also reported good agreement of the mDC model for mono- and divalent salt solutions for polymer-based polyelectrolyte ligands.[26]

The capability to reliably predict the ssDNA brush height will pave the way for engineering DNA-NP crystals with lattice-dependent and distance-dependent properties in high salt concentration environments including multivalent counterions, for applications such as plasmon-based sensing and diagnostics. Furthermore, without the influence of Watson–Crick specific base-pairing, non-base-pairing DNA can serve as an excellent model polyelectrolyte with high monodispersity and length tunability for biophysical studies towards elucidating the interactions of polyelectrolyte brushes in more complex salt environments.

In summary, we have demonstrated that with non-base-pairing DNA as a ligand for nanoparticles, 2D nanoparticle monolayers with long-range crystalline order can be achieved in high IS solutions—conditions relevant to real-world sensing and diagnostic applications but typically prone to nanoparticle aggregation and successive precipitation. In addition, we presented a modified Daoud–Cotton model for predicting the brush height based on the ligand length and IS in $MgCl_2$ salt environments. The results presented in this study may also be further extended towards the crystallization of other nanoparticle systems (with different nanoparticle cores and/or polyelectrolyte brush ligands) in multivalent salt environments.

Received: August 13, 2013
Revised: November 5, 2013
Published online: December 20, 2013

Keywords: crystallization · divalent salts · DNA hybridization · DNA nanoparticles · DNA nanotechnology

[1] S. Y. Park, A. K. R. Lytton-Jean, B. Lee, S. Weigand, G. C. Schatz, C. A. Mirkin, *Nature* **2008**, *451*, 553 – 556.
[2] D. Nykypanchuk, M. M. Maye, D. van der Lelie, O. Gang, *Nature* **2008**, *451*, 549 – 552.
[3] M. R. Jones, R. J. Macfarlane, B. Lee, J. Zhang, K. L. Young, A. J. Senesi, C. A. Mirkin, *Nat. Mater.* **2010**, *9*, 913 – 917.
[4] R. J. Macfarlane, B. Lee, M. R. Jones, N. Harris, G. C. Schatz, C. A. Mirkin, *Science* **2011**, *334*, 204 – 208.
[5] S. J. Tan, M. J. Campolongo, D. Luo, W. Cheng, *Nat. Nanotechnol.* **2011**, *6*, 268 – 276.
[6] J. I. Cutler, E. Auyeung, C. A. Mirkin, *J. Am. Chem. Soc.* **2012**, *134*, 1376 – 1391.
[7] G. P. Goodrich, M. R. Helfrich, J. J. Overberg, C. D. Keating, *Langmuir* **2004**, *20*, 10246 – 10251.
[8] J.-W. Keum, A. P. Hathorne, H. Bermudez, *Wiley Interdiscip. Rev. Nanomed. Nanobiotechnol.* **2011**, *3*, 282 – 297.
[9] W. Cheng, M. R. Hartman, D.-M. Smilgies, R. Long, M. J. Campolongo, R. Li, K. Sekar, C.-Y. Hui, D. Luo, *Angew. Chem.* **2010**, *122*, 390 – 394; *Angew. Chem. Int. Ed.* **2010**, *49*, 380 – 384.
[10] M. J. Campolongo, S. J. Tan, D.-M. Smilgies, M. Zhao, Y. Chen, I. Xhangolli, W. Cheng, D. Luo, *ACS Nano* **2011**, *5*, 7978 – 7985.
[11] N.-E. L. Saris, E. Mervaala, H. Karppanen, J. A. Khawaja, A. Lewenstam, *Clin. Chim. Acta* **2000**, *294*, 1 – 26.
[12] T. G. Martin, H. Dietz, *Nat. Commun.* **2012**, *3*, 1103.
[13] J. SantaLucia, D. Hicks, *Annu. Rev. Biophys. Biomol. Struct.* **2004**, *33*, 415 – 440.
[14] W. J. Parak, T. Pellegrino, C. M. Micheel, D. Gerion, S. C. Williams, A. P. Alivisatos, *Nano Lett.* **2003**, *3*, 33 – 36.
[15] T. Pellegrino, R. A. Sperling, A. P. Alivisatos, W. J. Parak, *BioMed Res. Internat.* **2008**, 2007.
[16] R. Jin, G. Wu, Z. Li, C. A. Mirkin, G. C. Schatz, *J. Am. Chem. Soc.* **2003**, *125*, 1643 – 1654.
[17] H. Chen, S. P. Meisburger, S. A. Pabit, J. L. Sutton, W. W. Webb, L. Pollack, *Proc. Natl. Acad. Sci. USA* **2012**, *109*, 799 – 804.
[18] Y. Liu, X.-M. Lin, Y. Sun, T. Rajh, *J. Am. Chem. Soc.* **2013**, *135*, 3764 – 3767.
[19] K. J. M. Bishop, C. E. Wilmer, S. Soh, B. A. Grzybowski, *Small* **2009**, *5*, 1600 – 1630.
[20] F. M. van der Kooij, D. van der Beek, H. N. W. Lekkerkerker, *J. Phys. Chem. B* **2001**, *105*, 1696 – 1700.
[21] E. K. Rideal, *An Introduction to Surface Chemistry*, Cambridge University Press, Cambridge, UK, **1926**.
[22] H. Y. Erbil, *Surface Chemistry of Solid and Liquid Interfaces*, Blackwell Publishing Ltd., Oxford, **2006**.
[23] R. Bahadur, L. M. Russell, S. Alavi, *J. Phys. Chem. B* **2007**, *111*, 11989 – 11996.
[24] N. Matubayasi, H. Matsuo, K. Yamamoto, S. Yamaguchi, A. Matuzawa, *J. Colloid Interface Sci.* **1999**, *209*, 398 – 402.
[25] S. J. Hurst, A. K. R. Lytton-Jean, C. A. Mirkin, *Anal. Chem.* **2006**, *78*, 8313 – 8318.
[26] X. Guo, M. Ballauff, *Phys. Rev. E* **2001**, *64*, 051406-1 – 051406-9.

